JACS
JOURNAL OF THE AMERICAN CHEMICAL SOCIETY
pubs.acs.org/JACS
Article

Macrocyclic Ligands with an Unprecedented Size-Selectivity Pattern for the Lanthanide Ions

Aohan Hu, Samantha N. MacMillan, and Justin J. Wilson*

Cite This: J. Am. Chem. Soc. 2020, 142, 13500−13506
Read Online

ACCESS | Metrics & More | Article Recommendations | Supporting Information

ABSTRACT: Lanthanides (Ln^{3+}) are critical materials used for many important applications, often in the form of coordination compounds. Tuning the thermodynamic stability of these compounds is a general concern, which is not readily achieved due to the similar coordination chemistry of lanthanides. Herein, we report two 18-membered macrocyclic ligands called macrodipa and macrotripa that show for the first time a dual selectivity toward both the light, large Ln^{3+} ions and the heavy, small Ln^{3+} ions, as determined by potentiometric titrations. The lanthanide complexes of these ligands were investigated by NMR spectroscopy and X-ray crystallography, which revealed the occurrence of a significant conformational toggle between a 10-coordinate Conformation A and an 8-coordinate Conformation B that accommodates Ln^{3+} ions of different sizes. The origin of this selectivity pattern was further supported by density functional theory (DFT) calculations, which show the complementary effects of ligand strain energy and metal−ligand binding energy that contribute to this conformational switch. This work demonstrates how novel ligand design strategies can be applied to tune the selectivity pattern for the Ln^{3+} ions.

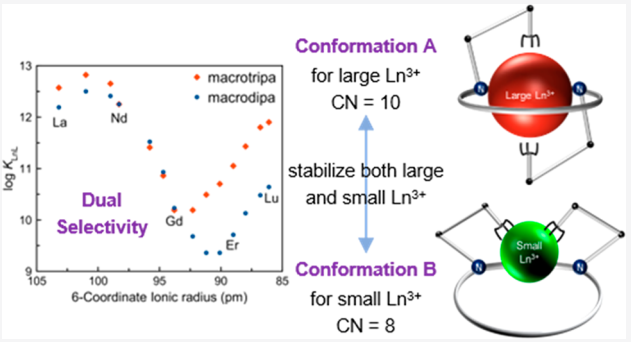

INTRODUCTION

The unique physical properties of the lanthanides (Ln^{3+}) are critical for use in magnets, superconductors, catalysts, luminescent phosphors, and medicinal agents.[1−6] Despite their diverse magnetic and electronic properties, Ln^{3+} ions possess similar chemical properties dictated by their strong preference for the +3 oxidation state and tendency to engage in ionic bonding.[7,8] The major distinguishing feature among them is their ionic radius, which decreases across the series, a phenomenon known as the lanthanide contraction.[9]

For many applications of the Ln^{3+}, a ligand is required to chelate these ions to control and modify their chemical properties. The availability of a range of chelators with different affinities and selectivity patterns for the Ln^{3+} ions, measured by the stability constant K_{LnL}, is valuable for their implementation.[10] Generally, most ligands possess a higher affinity for the heavier, smaller Ln^{3+} ions because the increased charge density on these smaller ions enhances metal−ligand electrostatic interactions.[11] Recent ligand design efforts, however, have led to systems with other Ln^{3+}-selectivity patterns. To date, three types of selectivity patterns have been identified (Figure 1). As noted above, the most common trend shows a systematic increase in K_{LnL} across the lanthanide series (type I). This type I behavior is observed for many well-known ligands including EDTA[12] (Figure 1 and Chart 1), 1,4,7,10-tetraazacyclododecane-1,4,7,10-tetraacetic acid (DOTA),[13] and diethylenetriamine-pentaacetic acid (DTPA).[14,15]

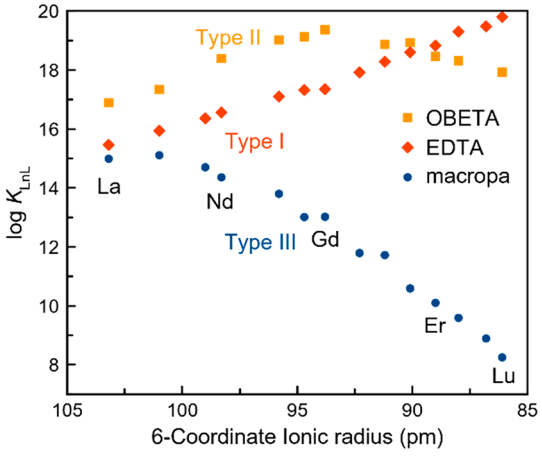

Figure 1. Stability constants of Ln^{3+} complexes formed with EDTA, OBETA, and macropa plotted versus ionic radii.

Received: May 12, 2020
Published: July 22, 2020

https://dx.doi.org/10.1021/jacs.0c05217
J. Am. Chem. Soc. 2020, 142, 13500−13506

Chart 1. Structures of Ligands Discussed in This Work

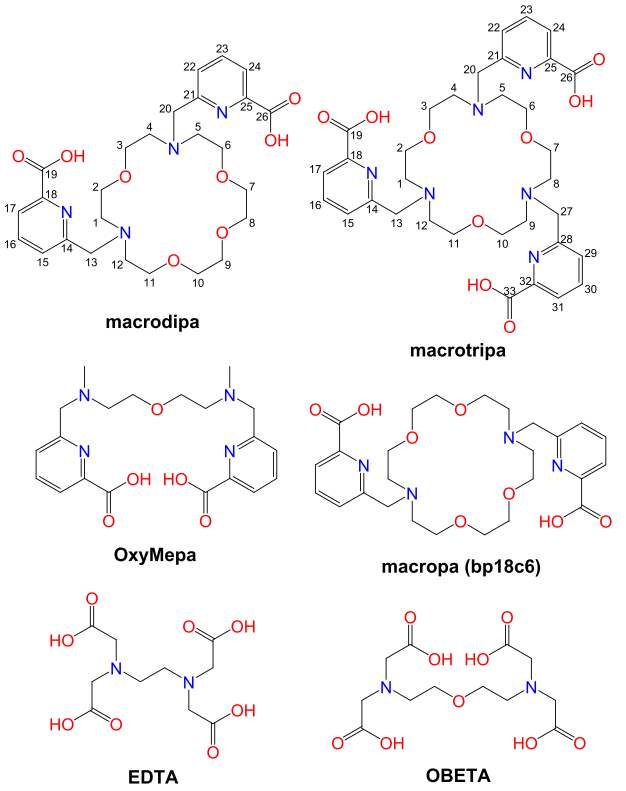

Another less frequently observed trend, type II, has the stability reach a maximum prior to dropping again. The ligands OBETA[16,17] (Figure 1 and Chart 1) and 1,4,7,10-tetrakis-(carbamoylmethyl)-1,4,7,10-tetraazacyclododecane (TCMC)[18] follow this pattern. The rarely observed behavior, type III, occurs with ligands having reverse-size selectivity, an unusual thermodynamic preference for large over small Ln^{3+} ions. This pattern has been observed in ligands containing the large diaza-18-crown-6 macrocycle, such as macropa[19] (Figure 1 and Chart 1) and 1,10-diaza-4,7,13,16-tetraoxacyclooctadecane-*N*,*N*′-diacetic acid (dacda).[20] A common feature of these three selectivity patterns is that they all have a maximum affinity for only one Ln^{3+} ion.

Inspired by macropa and our ongoing research efforts on chelating agents for large metal ions of biomedical and industrial relevance,[21−24] we sought to explore other ligands containing 18-membered macrocycles. Specifically, we investigated an isomer of macropa, called macrodipa, and a triaza-18-crown-6 ligand[25,26] bearing three pendent picolinate donors, macrotripa (Chart 1). Notably, these macrocycles are cyclic analogues of the previously reported ligand OxyMepa[27] (Chart 1) that provides a similar albeit truncated set of donor atoms. Over the course of our studies on their Ln^{3+} coordination chemistry, we found that macrodipa and macrotripa undergo dramatic conformational changes upon binding large versus small ions. These conformational changes manifest in a previously unreported type IV selectivity pattern with one minimum and two maxima of stability across the Ln^{3+} series. This work demonstrates how novel ligand design strategies can be employed to differentiate these ions in new ways.

RESULTS AND DISCUSSION

The syntheses of macrodipa and macrotripa (Schemes S1 and S2) involve the assembly of the tosyl-protected 18-crown-6 macrocycles, deprotection of the tosyl groups, and subsequent alkylation of the picolinate donor arms. They were characterized by NMR spectroscopy, mass spectrometry, and HPLC (Figures S1−S10).

Potentiometric titrations were performed to determine their protonation constants (K_i, Table S1). To probe the thermodynamic affinities of these ligands for Ln^{3+} ions, we conducted potentiometric titrations to obtain their stability constants (K_{LnL} and K_{LnHL}, Table 1). These protonation and stability constants are defined in eqs 1−3, with the concentrations of all species at chemical equilibrium.

$$K_i = [H_iL]/[H^+][H_{i-1}L] \quad (1)$$

$$K_{LnL} = [LnL]/[Ln^{3+}][L] \quad (2)$$

$$K_{LnHL} = [LnHL]/[H^+][LnL] \quad (3)$$

Table 1. Stability Constants of the Lanthanide Complexes Formed with Macrodipa, Macrotripa, OxyMepa, Macropa, EDTA, and OBETA

	macrodipa[a]	macrotripa[a]		OxyMepa[b]	macropa[c]		EDTA[d]	OBETA[e]
Ln^{3+}	log K_{LnL}	log K_{LnL}	log K_{LnHL}	log K_{LnL}	log K_{LnL}	log K_{LnHL}	log K_{LnL}	log K_{LnL}
La^{3+}	12.19(2)	12.57(1)	3.67(2)	9.93	14.99	2.28	15.46	16.89
Ce^{3+}	12.50(4)	12.82(2)	3.66(4)	10.74	15.11	2.07	15.94	17.34
Pr^{3+}	12.41(2)	12.65(1)	3.65(2)	11.25	14.70	2.96	16.36	
Nd^{3+}	12.25(3)	12.25(2)	3.88(1)	11.49	14.36	2.08	16.56	18.39
Sm^{3+}	11.52(2)	11.41(1)	3.99(1)	12.13	13.80	2.70	17.10	19.02
Eu^{3+}	10.93(1)	10.86(1)	4.24(2)	12.15	13.01	1.97	17.32	19.13
Gd^{3+}	10.23(2)	10.19(2)	4.51(1)	12.02	13.02	2.48	17.35	19.37
Tb^{3+}	9.68 (1)	10.19(2)	4.82(1)	12.17	11.79	2.91	17.92	
Dy^{3+}	9.36(2)	10.49(3)	4.86(2)	12.18	11.72	2.42	18.28	18.87
Ho^{3+}	9.36(1)	10.70(3)	4.90(1)	12.10	10.59		18.60	18.93
Er^{3+}	9.71(4)	11.05(3)	4.92(4)	12.00	10.10		18.83	18.46
Tm^{3+}	10.13(1)	11.43(5)	4.89(2)	12.05	9.59		19.30	
Yb^{3+}	10.48(1)	11.80(3)	4.88(1)	12.14	8.89		19.48	18.31
Lu^{3+}	10.64(4)	11.90(1)	4.93(2)	12.21	8.25		19.80	17.93

[a]0.1 M KCl, this work. The values in the parentheses are one standard deviation of the last significant figure. [b]0.1 M KCl, ref 27. [c]0.1 M KCl, ref 19. [d]0.1 M ionic strength, ref 12. [e]0.1 M KCl, refs 16 and 17.

https://dx.doi.org/10.1021/jacs.0c05217
J. Am. Chem. Soc. 2020, 142, 13500−13506

Figure 2 shows a plot of log K_{LnL} versus the Ln^{3+} ionic radius[28] for both macrodipa and macrotripa, which reveals them to be the

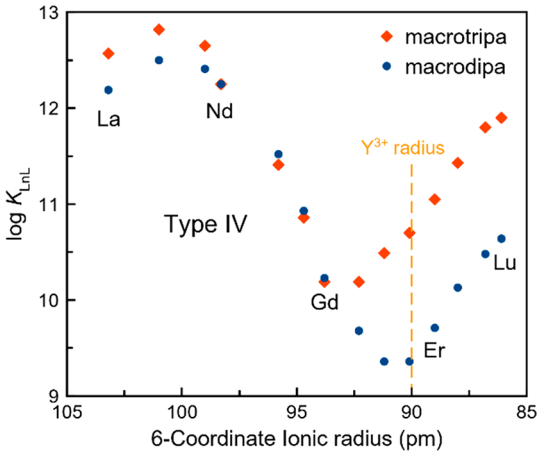

Figure 2. Stability constants of Ln^{3+} complexes formed with macrodipa and macrotripa plotted versus ionic radii.

first known ligands that exhibit type IV selectivity. In comparing the log K_{LnL} values between Ln^{3+}-macrodipa and Ln^{3+}-macrotripa systems, they are similar for early lanthanides, La^{3+}–Gd^{3+}. Ln^{3+}-macrodipa reaches a minimum for Dy^{3+} and Ho^{3+}, whereas for macrotripa the minimum occurs earlier in the series, between Gd^{3+} and Tb^{3+}. For late lanthanides, the macrotripa complexes are significantly more stable than those of macrodipa.

The log K_{LnHL} values, which represent the protonation of LnL complex, are also noteworthy. These values were not found for Ln^{3+}-macrodipa complexes but were observed for Ln^{3+}-macrotripa complexes. Comparing the chemical structures of macrodipa and macrotripa and their complexes (vide infra), it can be reasonably inferred that this protonation event occurs on the third picolinate arm in macrotripa. The K_{LnHL} values of the macrotripa complexes remain steady from La^{3+} to Pr^{3+}, but then increase abruptly from Nd^{3+} to Tb^{3+}, before leveling off from Dy^{3+} to Lu^{3+}. The sudden change in log K_{LnHL} implies that a conformational change may be present for Ln^{3+}-macrotripa complexes when crossing the Ln^{3+} series.

To gain insight on the type IV selectivity of macrodipa and macrotripa, we analyzed their complexes of the largest and smallest lanthanides, La^{3+} and Lu^{3+}, by NMR spectroscopy. These diamagnetic La^{3+} and Lu^{3+} complexes were characterized by ^{1}H, $^{13}C\{^{1}H\}$, and 2D (HSQC, HMBC, COSY, ROESY) NMR spectroscopy in D_2O at pD = 7 (Figures 3 and S41–S80). The ^{1}H NMR spectra of all four complexes indicate that a single species is present in solution. However, significant differences are apparent in comparing the La^{3+} and Lu^{3+} complexes. For example, the La^{3+}-macrodipa complex is 2-fold symmetric, indicated by one-half the number of ^{1}H and ^{13}C resonances relative to the asymmetric Lu^{3+}-macrodipa complex.

Additionally, the hydrogen resonances from the methylene groups linking the crown and picolinate donors (H-13, H-20 for macrodipa, and H-13, H-20, H-27 for macrotripa; Chart 1), which are informative due to their proximities to the picolinate donors, are significantly different between the La^{3+} and Lu^{3+} complexes. For example, the peaks for the diastereotopic H-27′ and H-27″ in the La^{3+}-macrotripa case are well-separated,

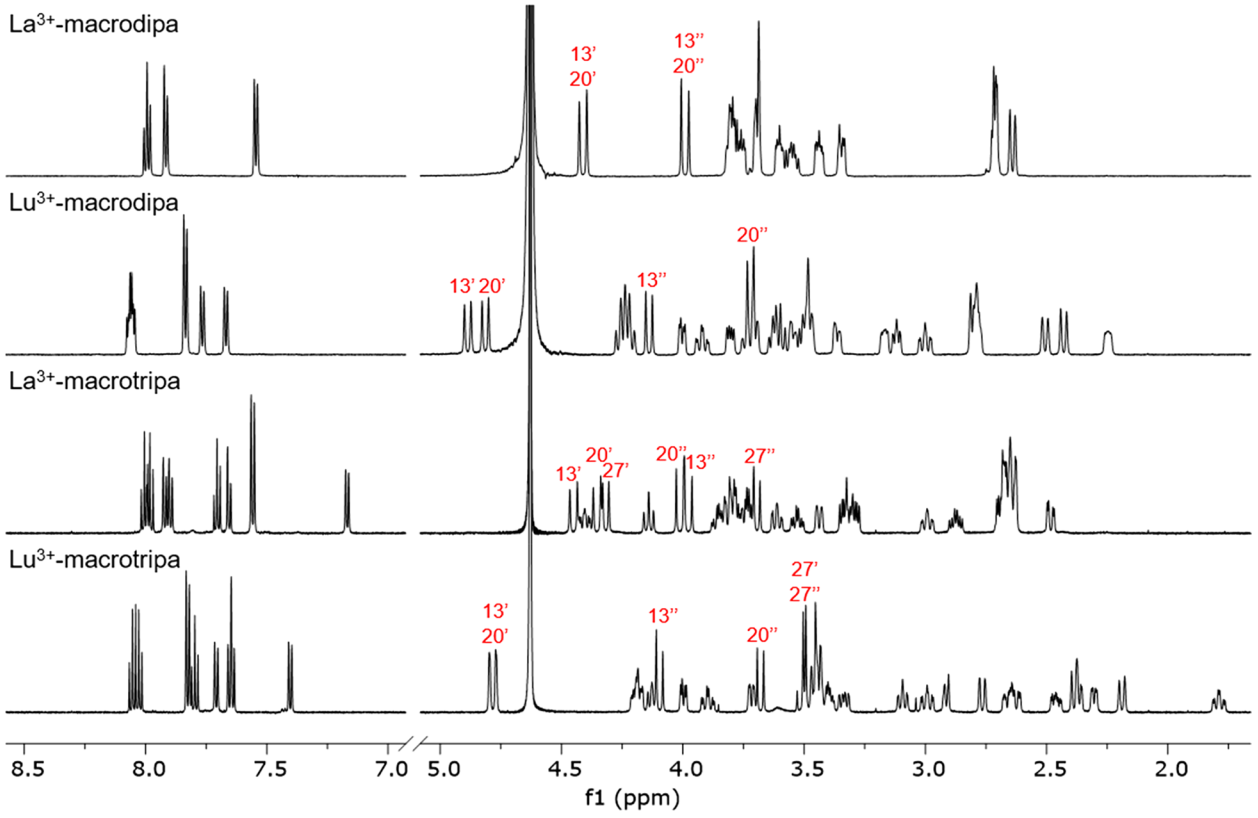

Figure 3. ^{1}H NMR spectra of macrodipa and macrotripa complexes formed with La^{3+} and Lu^{3+} (600 MHz, D_2O, pD = 7, 25 °C). Selected peaks are labeled using the numbering scheme in Chart 1.

https://dx.doi.org/10.1021/jacs.0c05217
J. Am. Chem. Soc. 2020, 142, 13500−13506

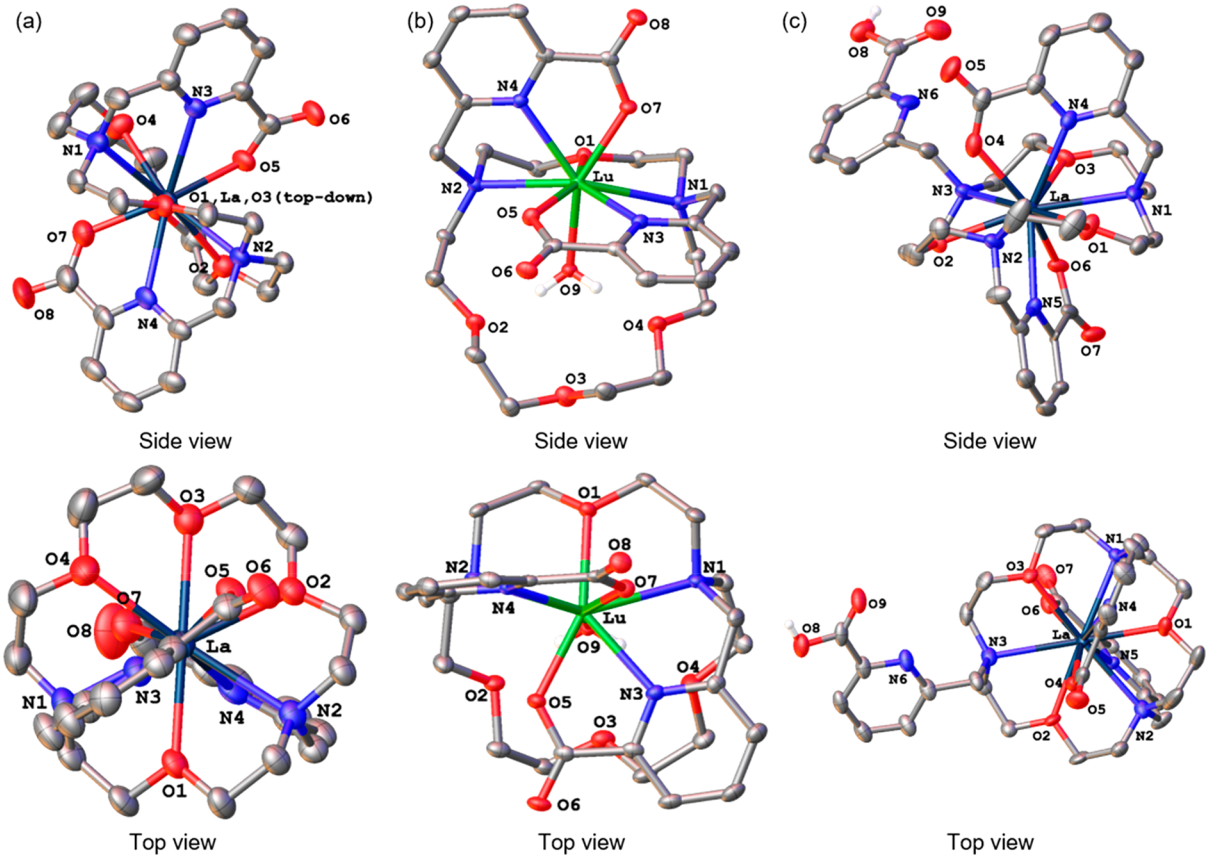

Figure 4. Crystal structures of (a) $[La(macrodipa)]^+$, (b) $[Lu(macrodipa)(OH_2)]^+$, and (c) $[La(macrotripa)]^+$ complexes. Thermal ellipsoids are drawn at the 50% probability level. Solvent, counterions, and nonacidic hydrogen atoms are omitted for clarity. Only one of the two $[La(macrodipa)]^+$ complexes in the asymmetric unit is shown.

whereas for Lu^{3+}-macrotripa they have near-identical chemical shifts. Collectively, these NMR data suggest that there is a significant conformational difference between the La^{3+} and Lu^{3+} complexes of these ligands.

To further explore these different conformations, we characterized these complexes by X-ray crystallography. Crystal structures of $[La(macrodipa)]^+$, $[Lu(macrodipa)(OH_2)]^+$, and $[La(macrotripa)]^+$ are shown in Figure 4. A weakly diffracting and partially twinned crystal of $[Lu(macrotripa)(OH_2)]$ was also obtained, but the connectivity information was reliably ascertained (Figure S89). Confirming the NMR spectroscopic data, the La^{3+} complexes attain a significantly different conformation than do the Lu^{3+} complexes. In both La^{3+} structures, this ion is encapsulated into the 18-membered macrocyclic core, which interacts with all of its six donor atoms. Moreover, the pendent picolinate groups bind to La^{3+} from two opposite faces of the macrocycle, resulting in 10-coordinate complexes. The third picolinate donor of macrotripa does not participate in coordination. Consistent with its NMR spectra, $[La(macrodipa)]^+$ attains a slightly distorted C_2 symmetry. By contrast, both Lu^{3+} structures show significantly different coordination environments. Specifically, only two tertiary nitrogens and one ethereal oxygen from the macrocycle act as donors. The coordination sphere is completed with the four donor atoms from two picolinate groups and an inner-sphere water molecule, yielding 8-coordinate Lu^{3+} centers. In $[Lu(macrotripa)(OH_2)]$, the third unbound picolinate donor is positioned to interact with the bound water molecule through hydrogen bonding. Except for the macrocycle, these Lu^{3+} structures are highly comparable to those found for the acyclic ligand OxyMepa,[27] which displays type I selectivity, indicating that the complete 18-crown-6 macrocycles of macrodipa and macrotripa are critical for their unique Ln^{3+}-selectivity profiles.

As a further validation on the proposed intramolecular hydrogen bond in $[Lu(macrotripa)(OH_2)]$, we optimized its structure (Figure S98) using validated DFT methods (vide infra) and carried out a topological analysis of the electron density using the quantum theory of atoms in molecules (QTAIM).[29] Specifically, we found all bond critical points (BCP) with the *Multiwfn*[30] program (Figure S99). A BCP was located between a hydrogen atom of the coordinated water molecule and the oxygen atom of the pendent picolinate group. At this BCP, the magnitude of its local electron density (ρ) is 0.079 au, and the Laplacian of the electron density ($\nabla^2\rho$) is 0.16 au. The positive value for $\nabla^2\rho$ reflects a closed-shell hydrogen bond, and the magnitude of ρ suggests that this interaction is strong, comparable to that found between OH^- and H_2O.[31−33] This analysis supports the proposed intramolecular hydrogen-bonding interaction present in $[Lu(macrotripa)(OH_2)]$.

On the basis of the NMR and X-ray crystallographic data, it is clear that macrodipa and macrotripa attain distinct conformations depending on whether they bind large or small Ln^{3+} ions (Scheme 1). Large ions, like La^{3+}, attain Conformation A, in which the ion is fully encapsulated by the macrocycle, whereas small ions, like Lu^{3+}, sit in Conformation B, held by only part of the macrocycle. The ability of these ligands to drastically alter their conformations to match the sizes of metal ions accounts for the type IV selectivity pattern. The structures may also explain

https://dx.doi.org/10.1021/jacs.0c05217
J. Am. Chem. Soc. 2020, 142, 13500−13506

Scheme 1. Depiction of the Conformational Toggle Present in Ln^{3+}-Macrodipa and Ln^{3+}-Macrotripa Complex Systems

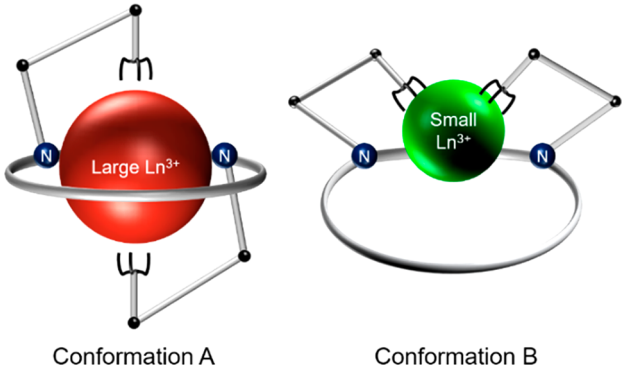

the difference in thermodynamic stability of macrodipa and macrotripa for the late, but not early, Ln^{3+} (Figure 2). Both ligands give rise to identical coordination spheres for the large early lanthanides, like La^{3+}, and therefore exhibit only minor differences in their thermodynamic stabilities. However, for the small late lanthanides, like Lu^{3+}, the inner coordination spheres are nearly identical between macrodipa and macrotripa, but the outer sphere differs due to the hydrogen-bonding interaction with the coordinated water molecule. Thus, the differences in thermodynamic stability between the macrodipa and macrotripa complexes of the late lanthanides are most likely a consequence of the hydrogen bonding of the pendent picolinate donor arm. This result highlights how modifying the outer coordination sphere of lanthanide complexes fine-tunes their thermodynamic properties.

As a further test of this conformational toggle, we investigated the complexes of Y^{3+}, a diamagnetic Ln^{3+} analogue with an ionic radius comparable to that of Ho^{3+},[7,28] by NMR spectroscopy. The ^1H and $^{13}C\{^1H\}$ NMR spectra of Y^{3+}-macrodipa and Y^{3+}-macrotripa were acquired in D_2O at pD = 7 (Figures S81−S88). Both Conformations A and B are detected for Y^{3+}-macrodipa, in a molar ratio of 1:15. For the Y^{3+}-macrotripa complex, only Conformation B is observed. The 90-pm ionic radius of Y^{3+} places its macrodipa complex near the local minimum of log K_{LnL}, but its macrotripa complex is placed rather far from the minimum (Figure 2). Thus, these NMR data show that the conformational switch occurs for complexes of ions with their radii near the minimum of stability; larger and smaller ions show preferences for Conformations A and B, respectively.

DFT has been extensively used to investigate the properties of Ln^{3+} coordination compounds.[34−36] In this study, we took advantage of this powerful tool to help understand the origin of the type IV selectivity pattern of these ligands. We focused exclusively on the Ln^{3+}-macrodipa system. These complexes lack the third noncoordinated picolinate arm of the Ln^{3+}-macrotripa and therefore provide a straightforward system to model the inner coordination spheres of these complexes. DFT calculations were executed using *Gaussian 09*[37] with the ωB97XD functional.[38,39] This functional, which is long-range corrected and includes dispersion corrections, has been shown to give accurate geometries of Ln^{3+} complexes.[40] Because of the importance of relativistic effects in Ln^{3+} ions,[41] we used the large-core relativistic effective core potential (LCRECP) by Dolg[42] to account for these effects in a computationally efficient manner. For light atoms, the 6-31G(d,p) basis set[43,44] was applied. The SMD solvation model[45,46] was implemented to take the solvent effects into consideration. The ΔG° for the conformational equilibrium:

$$[Ln(macrodipa)]^+ \text{ (Conformation A, } aq) + H_2O\ (l) \rightleftharpoons [Ln(macrodipa)(OH_2)]^+ \text{ (Conformation B, } aq) \quad (4)$$

was calculated for Ln^{3+}-macrodipa complexes. The ΔG° (Figure 5) is positive for light Ln^{3+} and negative for heavy Ln^{3+}. This

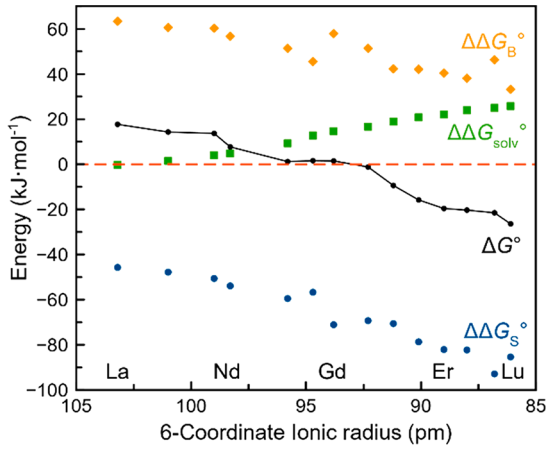

Figure 5. DFT-computed standard free energies for the conformational equilibrium (eq 4) of Ln^{3+}-macrodipa complexes.

observation is consistent with the experimental results with La^{3+}-macrodipa and Lu^{3+}-macrodipa complexes attaining Conformations A and B, respectively. Additionally, ΔG° changes its sign between Gd^{3+} and Tb^{3+}, which indicates the switch of favored conformation. This crossover suggests that the type IV behavior of macrodipa is a consequence of the significant conformational changes that occur when binding Ln^{3+} ions of different sizes.

Furthermore, ΔG° for this conformational change can be broken into three contributors. Specifically, it can be expressed as the sum of the relative ligand strain energies ($\Delta\Delta G_S^\circ$), relative metal−ligand binding energies ($\Delta\Delta G_B^\circ$), and relative solvation energies ($\Delta\Delta G_{solv}^\circ$) between Conformations A and B, as described in the Supporting Information. As shown in Figure 5, $\Delta\Delta G_{solv}^\circ$ is positive for all Ln^{3+} complexes, which reveals that Conformer A and the noncoordinated water ligand are better solvated in aqueous solution than is Conformer B. Likewise, $\Delta\Delta G_B^\circ$ is positive for all Ln^{3+}, which indicates that Conformation A is better suited to neutralize the electrostatic charges of these ions than is Conformation B. This observation can be rationalized by the fact that Conformation A interacts with the Ln^{3+} with two more donor atoms. However, $\Delta\Delta G_B^\circ$ decreases as the Ln^{3+} gets smaller, which suggests that Conformation A is less effective at binding the smaller ions. By contrast, $\Delta\Delta G_S^\circ$ is negative across the entire series, which shows that Conformation B requires less ligand strain than does Conformation A. Among the three values, $\Delta\Delta G_S^\circ$ shows the most significant changes as a function of the Ln^{3+} ionic radius, and it becomes more negative for smaller ions. Importantly, the strain energy is the only exothermic term for the switch from Conformation A to B, and thus it is the driving factor in the conformational switch of macrodipa. This result suggests that modifications of this ligand scaffold to alter the strain energy term could lead to a significant shift in the Ln^{3+}-stability pattern for this ligand class.

https://dx.doi.org/10.1021/jacs.0c05217
J. Am. Chem. Soc. 2020, 142, 13500−13506

CONCLUSION

In summary, this work describes two ligands that display an unprecedented type IV selectivity pattern with one minimum and two maxima of K_{LnL} across the Ln^{3+} series. This novel selectivity pattern may have key applications in Ln^{3+} separations and nuclear medicine, where it is often desirable to stably chelate a range of metal ions with disparate ionic radii. Our structural data by NMR spectroscopy and X-ray crystallography show that both macrodipa and macrotripa undergo a significant conformational shift in moving from a large to small Ln^{3+} ion, which allows for high thermodynamic stability for both early and late Ln^{3+}. In comparing macrodipa and macrotripa, we have shown that one can modify these ligands to tune the position of the minimum and the overall magnitude of thermodynamic stability. Our DFT calculations further support the presence of this conformational toggle and show that the ligand strain and metal−ligand binding energies are complementary factors contributing to the conformational switch. Between them, we believe that the ligand strain energy is more easily modified, for example, by including groups in the macrocyclic backbone that prevent conformational flexibility, which thus presents a path for tuning these ligands for different applications. This work demonstrates how the incorporation of conformational flexibility in ligands can be used to satisfy the coordination environments of different metal ions, a principle of great value for chelator design efforts.

ASSOCIATED CONTENT

Supporting Information

The Supporting Information is available free of charge at https://pubs.acs.org/doi/10.1021/jacs.0c05217.

Experimental procedures and supplementary data for chemical synthesis, potentiometric titrations, NMR spectroscopy studies, X-ray crystallography, and DFT calculations (PDF)

Geometry outputs for all DFT-optimized structures (ZIP)

Crystallographic data for La^{3+}-macrodipa, Lu^{3+}-macrodipa, and La^{3+}-macrotripa complexes (CIF)

AUTHOR INFORMATION

Corresponding Author

Justin J. Wilson − *Department of Chemistry and Chemical Biology, Cornell University, Ithaca, New York 14853, United States;* orcid.org/0000-0002-4086-7982; Email: jjw275@cornell.edu

Authors

Aohan Hu − *Department of Chemistry and Chemical Biology, Cornell University, Ithaca, New York 14853, United States;* orcid.org/0000-0002-9720-3159

Samantha N. MacMillan − *Department of Chemistry and Chemical Biology, Cornell University, Ithaca, New York 14853, United States;* orcid.org/0000-0001-6516-1823

Complete contact information is available at: https://pubs.acs.org/10.1021/jacs.0c05217

Notes

The authors declare no competing financial interest.

ACKNOWLEDGMENTS

This research was supported in part by seed funding from the Academic Integration grant program at Cornell University and from the College of Arts and Sciences at Cornell University and by the National Institute of Biomedical Imaging and Bioengineering of the National Institutes of Health under award number R21EB027282. The content is solely the responsibility of the authors and does not necessarily represent the official views of the National Institutes of Health. This research was also supported by a Cottrell Research Scholar Award from the Research Corporation for Science Advancement. This research made use of the NMR Facility at Cornell University, which is supported, in part, by the U.S. National Science Foundation under award number CHE-1531632.

REFERENCES

(1) Cheisson, T.; Schelter, E. J. Rare Earth Elements: Mendeleev's Bane, Modern Marvels. *Science* **2019**, *363*, 489−493.

(2) Woodruff, D. N.; Winpenny, R. E. P.; Layfield, R. A. Lanthanide Single-Molecule Magnets. *Chem. Rev.* **2013**, *113*, 5110−5148.

(3) Dos santos-García, A. J.; Alario-Franco, M. A.; Sáez-Puche, R. The Rare Earth Elements: Superconducting Materials. *Encyclopedia of Inorganic and Bioinorganic Chemistry*; John Wiley & Sons, Ltd.: Chichester, UK, 2012.

(4) Pellissier, H. Recent Developments in Enantioselective Lanthanide-Catalyzed Transformations. *Coord. Chem. Rev.* **2017**, *336*, 96−151.

(5) Qin, X.; Liu, X.; Huang, W.; Bettinelli, M.; Liu, X. Lanthanide-Activated Phosphors Based on 4f-5d Optical Transitions: Theoretical and Experimental Aspects. *Chem. Rev.* **2017**, *117*, 4488−4527.

(6) Teo, R. D.; Termini, J.; Gray, H. B. Lanthanides: Applications in Cancer Diagnosis and Therapy. *J. Med. Chem.* **2016**, *59*, 6012−6024.

(7) Cotton, S. A. Scandium, Yttrium & the Lanthanides: Inorganic & Coordination Chemistry. *Encyclopedia of Inorganic Chemistry*; John Wiley & Sons, Ltd.: Chichester, UK, 2006.

(8) Huang, C.; Bian, Z. Introduction. In *Rare Earth Coordination Chemistry: Fundamentals and Applications*; Huang, C., Ed.; John Wiley & Sons (Asia) Pte Ltd.: Singapore, 2010; pp 1−39.

(9) Seitz, M.; Oliver, A. G.; Raymond, K. N. The Lanthanide Contraction Revisited. *J. Am. Chem. Soc.* **2007**, *129*, 11153−11160.

(10) Peters, J. A.; Djanashvili, K.; Geraldes, C. F. G. C.; Platas-Iglesias, C. The Chemical Consequences of the Gradual Decrease of the Ionic Radius along the Ln-Series. *Coord. Chem. Rev.* **2020**, *406*, 213146.

(11) Piguet, C.; Bünzli, J.-C. G. Mono- and Polymetallic Lanthanide-Containing Functional Assemblies: A Field between Tradition and Novelty. *Chem. Soc. Rev.* **1999**, *28*, 347−358.

(12) Martell, A. E.; Smith, R. M. *Critical Stability Constants*; Plenum Press: New York, 1974; Vol. *1*.

(13) Cacheris, W. P.; Nickle, S. K.; Sherry, A. D. Thermodynamic study of Lanthanide Complexes of 1,4,7-Triazacyclononane-*N*,*N*′,*N*″-triacetic Acid and 1,4,7,10-Tetraazacyclododecane-*N*,*N*′,*N*″,*N*‴-tetra-acetic Acid. *Inorg. Chem.* **1987**, *26*, 958−960.

(14) Moeller, T.; Thompson, L. C. Observations on the Rare Earths—LXXV: The Stabilities of Diethylenetriaminepentaacetic Acid Chelates. *J. Inorg. Nucl. Chem.* **1962**, *24*, 499−510.

(15) Grimes, T. S.; Nash, K. L. Acid Dissociation Constants and Rare Earth Stability Constants for DTPA. *J. Solution Chem.* **2014**, *43*, 298−313.

(16) Baranyai, Z.; Botta, M.; Fekete, M.; Giovenzana, G. B.; Negri, R.; Tei, L.; Platas-Iglesias, C. Lower Ligand Denticity Leading to Improved Thermodynamic and Kinetic Stability of the Gd^{3+} Complex: The Strange Case of OBETA. *Chem. - Eur. J.* **2012**, *18*, 7680−7685.

(17) Negri, R.; Baranyai, Z.; Tei, L.; Giovenzana, G. B.; Platas-Iglesias, C.; Bényei, A. C.; Bodnár, J.; Vágner, A.; Botta, M. Lower Denticity Leading to Higher Stability: Structural and Solution Studies of Ln(III)−OBETA Complexes. *Inorg. Chem.* **2014**, *53*, 12499−12511.

(18) Voss, D. A., Jr.; Farquhar, E. R.; Horrocks, W. D., Jr.; Morrow, J. R. Lanthanide(III) Complexes of Amide Derivatives of DOTA Exhibit an Unusual Variation in Stability across the Lanthanide Series. *Inorg. Chim. Acta* **2004**, *357*, 859−863.

(19) Roca-Sabio, A.; Mato-Iglesias, M.; Esteban-Gómez, D.; Tóth, É.; de Blas, A.; Platas-Iglesias, C.; Rodríguez-Blas, T. Macrocyclic Receptor Exhibiting Unprecedented Selectivity for Light Lanthanides. *J. Am. Chem. Soc.* **2009**, *131*, 3331−3341.
(20) Chang, C. A.; Rowland, M. E. Metal Complex Formation with 1,10-Diaza-4,7,13,16-tetraoxacyclooctadecane-*N*,*N*′-diacetic Acid. An Approach to Potential Lanthanide Ion Selective Reagents. *Inorg. Chem.* **1983**, *22*, 3866−3869.
(21) Thiele, N. A.; Brown, V.; Kelly, J. M.; Amor-Coarasa, A.; Jermilova, U.; MacMillan, S. N.; Nikolopoulou, A.; Ponnala, S.; Ramogida, C. F.; Robertson, A. K. H.; Rodríguez-Rodríguez, C.; Schaffer, P.; Williams, C., Jr.; Babich, J. W.; Radchenko, V.; Wilson, J. J. An Eighteen-Membered Macrocyclic Ligand for Actinium-225 Targeted Alpha Therapy. *Angew. Chem., Int. Ed.* **2017**, *56*, 14712−14717.
(22) Thiele, N. A.; MacMillan, S. N.; Wilson, J. J. Rapid Dissolution of $BaSO_4$ by Macropa, an 18-Membered Macrocycle with High Affinity for Ba^{2+}. *J. Am. Chem. Soc.* **2018**, *140*, 17071−17078.
(23) Thiele, N. A.; Woods, J. J.; Wilson, J. J. Implementing f-Block Metal Ions in Medicine: Tuning the Size Selectivity of Expanded Macrocycles. *Inorg. Chem.* **2019**, *58*, 10483−10500.
(24) Aluicio-Sarduy, E.; Thiele, N. A.; Martin, K. E.; Vaughn, B. A.; Devaraj, J.; Olson, A. P.; Barnhart, T. E.; Wilson, J. J.; Boros, E.; Engle, J. W. Establishing Radiolanthanum Chemistry for Targeted Nuclear Medicine Applications. *Chem. - Eur. J.* **2020**, *26*, 1238−1242.
(25) Chen, D.; Squattrito, P. J.; Martell, A. E.; Clearfield, A. Synthesis and Crystal Structure of a Nine-Coordinate Gadolinium(III) Complex of 1,7,13-Triaza-4,10,16-trioxacyclooctadecane-*N*,*N*′,*N*″-triacetic Acid. *Inorg. Chem.* **1990**, *29*, 4366−4368.
(26) Delgado, R.; Sun, Y.; Motekaitis, R. J.; Martell, A. E. Stabilities of Divalent and Trivalent Metal Ion Complexes of Macrocyclic Triazatriacetic Acids. *Inorg. Chem.* **1993**, *32*, 3320−3326.
(27) Hu, A.; Keresztes, I.; MacMillan, S. N.; Yang, Y.; Ding, E.; Zipfel, W. R.; DiStasio, R. A., Jr.; Babich, J. W.; Wilson, J. J. Oxyaapa: A Picolinate-Based Ligand with Five Oxygen Donors that Strongly Chelates Lanthanides. *Inorg. Chem.* **2020**, *59*, 5116−5132.
(28) Shannon, R. D. Revised Effective Ionic Radii and Systematic Studies of Interatomic Distances in Halides and Chalcogenides. *Acta Crystallogr., Sect. A: Found. Adv.* **1976**, *32*, 751−767.
(29) Bader, R. F. W. *Atoms in Molecules − A Quantum Theory*; Oxford University Press: Oxford, 1990.
(30) Lu, T.; Chen, F. Multiwfn: A Multifunctional Wavefunction Analyzer. *J. Comput. Chem.* **2012**, *33*, 580−592.
(31) Bader, R. F. W. A Quantum Theory of Molecular Structure and Its Applications. *Chem. Rev.* **1991**, *91*, 893−928.
(32) Grabowski, S. J.; Robinson, T. L.; Leszczynski, J. Strong Dihydrogen Bonds - ab initio and Atoms in Molecules Study. *Chem. Phys. Lett.* **2004**, *386*, 44−48.
(33) Parthasarathi, R.; Subramanian, V.; Sathyamurthy, N. Hydrogen Bonding without Borders: An Atoms-in-Molecules Perspective. *J. Phys. Chem. A* **2006**, *110*, 3349−3351.
(34) Tsipis, A. C. DFT Flavor of Coordination Chemistry. *Coord. Chem. Rev.* **2014**, *272*, 1−29.
(35) Platas-Iglesias, C.; Roca-Sabio, A.; Regueiro-Figueroa, M.; Esteban-Gómez, D.; de Blas, A.; Rodriguez-Blas, T. Applications of Density Functional Theory (DFT) to Investigate the Structural, Spectroscopic and Magnetic Properties of Lanthanide(III) Complexes. *Curr. Inorg. Chem.* **2011**, *1*, 91−116.
(36) Platas-Iglesias, C. The Solution Structure and Dynamics of MRI Probes Based on Lanthanide(III) DOTA as Investigated by DFT and NMR Spectroscopy. *Eur. J. Inorg. Chem.* **2012**, *2012*, 2023−2033.
(37) Frisch, M. J.; Trucks, G. W.; Schlegel, H. B.; Scuseria, G. E.; Robb, M. A.; Cheeseman, J. R.; Scalmani, G.; Barone, V.; Mennucci, B.; Petersson, G. A.; Nakatsuji, H.; Caricato, M.; Li, X.; Hratchian, H. P.; Izmaylov, A. F.; Bloino, J.; Zheng, G.; Sonnenberg, J. L.; Hada, M.; Ehara, M.; Toyota, K.; Fukuda, R.; Hasegawa, J.; Ishida, M.; Nakajima, T.; Honda, Y.; Kitao, O.; Nakai, H.; Vreven, T.; Montgomery, J. A., Jr.; Peralta, J. E.; Ogliaro, F.; Bearpark, M.; Heyd, J. J.; Brothers, E.; Kudin, K. N.; Staroverov, V. N.; Kobayashi, R.; Normand, J.; Raghavachari, K.; Rendell, A.; Burant, J. C.; Iyengar, S. S.; Tomasi, J.; Cossi, M.; Rega, N.; Millam, J. M.; Klene, M.; Knox, J. E.; Cross, J. B.; Bakken, V.; Adamo, C.; Jaramillo, J.; Gomperts, R.; Stratmann, R. E.; Yazyev, O.; Austin, A. J.; Cammi, R.; Pomelli, C.; Ochterski, J. W.; Martin, R. L.; Morokuma, K.; Zakrzewski, V. G.; Voth, G. A.; Salvador, P.; Dannenberg, J. J.; Dapprich, S.; Daniels, A. D.; Farkas, Ö.; Foresman, J. B.; Ortiz, J. V.; Cioslowski, J.; Fox, D. J. *Gaussian 09*, revision D.01; Gaussian, Inc.: Wallingford, CT, 2009.
(38) Chai, J.-D.; Head-Gordon, M. Systematic Optimization of Long-Range Corrected Hybrid Density Functionals. *J. Chem. Phys.* **2008**, *128*, 084106.
(39) Chai, J.-D.; Head-Gordon, M. Long-Range Corrected Hybrid Density Functionals with Damped Atom-Atom Dispersion Corrections. *Phys. Chem. Chem. Phys.* **2008**, *10*, 6615−6620.
(40) Roca-Sabio, A.; Regueiro-Figueroa, M.; Esteban-Gómez, D.; de Blas, A.; Rodríguez-Blas, T.; Platas-Iglesias, C. Density Functional Dependence of Molecular Geometries in Lanthanide(III) Complexes Relevant to Bioanalytical and Biomedical Applications. *Comput. Theor. Chem.* **2012**, *999*, 93−104.
(41) Barysz, M.; Ishikawa, Y. *Relativistic Methods for Chemists*; Springer Science+Business Media B.V.: Dordrecht, 2010.
(42) Dolg, M.; Stoll, H.; Savin, A.; Preuss, H. Energy-Adjusted Pseudopotentials for the Rare Earth Elements. *Theor. Chim. Acta* **1989**, *75*, 173−194.
(43) Hehre, W. J.; Ditchfield, R.; Pople, J. A. Self-Consistent Molecular Orbital Methods. XII. Further Extensions of Gaussian-Type Basis Sets for Use in Molecular Orbital Studies of Organic Molecules. *J. Chem. Phys.* **1972**, *56*, 2257−2261.
(44) Hariharan, P. C.; Pople, J. A. The Influence of Polarization Functions on Molecular Orbital Hydrogenation Energies. *Theor. Chim. Acta* **1973**, *28*, 213−222.
(45) Marenich, A. V.; Cramer, C. J.; Truhlar, D. G. Universal Solvation Model Based on Solute Electron Density and on a Continuum Model of the Solvent Defined by the Bulk Dielectric Constant and Atomic Surface Tensions. *J. Phys. Chem. B* **2009**, *113*, 6378−6396.
(46) Regueiro-Figueroa, M.; Esteban-Gómez, D.; de Blas, A.; Rodríguez-Blas, T.; Platas-Iglesias, C. Understanding Stability Trends along the Lanthanide Series. *Chem. - Eur. J.* **2014**, *20*, 3974−3981.

https://dx.doi.org/10.1021/jacs.0c05217
J. Am. Chem. Soc. 2020, 142, 13500−13506